journal

J. Am. Ceram. Soc., 93 [1] 155–160 (2010)
DOI: 10.1111/j.1551-2916.2009.03374.x

Synthesis and Characterization of Nanostructured Cerium Dioxide Thin Films Deposited by Ultrasonic Spray Pyrolysis

Mario F. García-Sánchez,[†,‡] Armando Ortiz,[‡] Guillermo Santana,[‡] Monserrat Bizarro,[‡] Juan Peña,[‡] Francisco Cruz-Gandarilla,[§] Miguel A. Aguilar-Frutis,[¶] and Juan C. Alonso[‡]

[‡]Instituto de Investigaciones en Materiales, Universidad Nacional Autónoma de México; Ciudad Universitaria, Coyoacán 04510, México D.F., México

[§]Escuela Superior de Física y Matemáticas, Instituto Politécnico Nacional; Edif. 9, U.P.A.L.M. 07738, México D.F., México

[¶]Centro de Investigación en Ciencia Aplicada y Tecnología Avanzada, Instituto Politécnico Nacional; Irrigación 11500, México D.F., México

Nanostructured thin films of cerium dioxide have been prepared on single-crystalline silicon substrates by ultrasonic spray pyrolysis using cerium acetylacetonate as a metal–organic precursor dissolved in anhydrous methanol and acetic acid as an additive. The morphology, structure, optical index, and electrical properties were studied by X-ray diffraction, scanning electron microscopy, atomic force microscopy, ellipsometry, and impedance spectroscopy. The use of additives is very important to obtain crack-free films. The substrate temperature and flow rate was optimized for obtaining smooth ($R_a < 0.4$ nm), dense ($n > 2$), and homogeneous nanocrystalline films with grain sizes as small as 10 nm. The influence of thermal annealing on the structural properties of films was studied. The low activation energy calculated for total conductivity (0.133 eV) is attributed to the nanometric size of the grains.

I. Introduction

Cerium dioxide (CeO_2) has been of great interest during the last years due to its multiple applications in several key areas of thin film technology. This material has a cubic fluorite-type crystal structure (lattice spacing 0.5411 nm) and combines a large bandgap (<3.5 eV) with a high dielectric constant ($\varepsilon \approx 26$), high ionic conductivity, and high-temperature stability.[1–8] Because of its chemical stability and close lattice parameter matching with silicon (0.35% lattice matching), CeO_2 has potential applicability in the area of optoelectronics: in silicon-on-insulator structures, stable capacitor devices for large-scale integration, photoelectrodes in dye-sensitized solar cells, and stable buffer layers between high-temperature superconducting materials and silicon substrates.[6–14] The high ionic conductivity has attracted great interest for applications such as gas sensors[15,16] and electrolyte or anode materials for intermediate-temperature solid oxide fuel cells (IT-SOFC).[17–28]

Several physical and chemical processes have been used to prepare CeO_2 thin films, including flash evaporation,[3] electron-beam evaporation,[4,5,9,15] spin coating,[1,2,16,23] sputtering,[6,29] MOCVD,[30] laser ablation,[31–33], and spray pyrolysis in its three versions: electrostatic, pneumatic, and ultrasonic.[7,11–14,18–20,33,34] Among them, the spray pyrolysis techniques are very attractive for the industry, because they allow the deposition of a wide variety of ceramic films over large areas with a simple process at low costs. Each one of the spray pyrolysis versions has advantages and drawbacks in terms of complexity and quality of the deposit.[35,36] Electrostatic spray deposition (ESD) has been used for preparing YSZ- and CeO_2-based films.[14,18,20,36,37] This technique produces almost monodispersed and fine drops; however, the effect of preferential landing of the charged droplets can lead to porous and/or cracked films. In pressurized spray deposition, there is less control on the microstructure of the deposited films due to a higher dispersion of droplet sizes.[38] However, it is reported as a more adequate technique to deposit dense films compared with the ESD technique. Ultrasonic spray deposition (USD) allows a smaller and homogeneous droplet size than electrostatic or pressurized spray,[35] and it has been widely used to prepare YSZ thin films.[35,39–41] In contrast, CeO_2 thin films have been produced only by Wang *et al.*[13] using USD. Anyway, in the three cases, the selection of precursors and the process of parameters' optimization have a great influence in the final properties of the films.

Nanostructured materials are characterized by unique physico-chemical properties with important applications. One of the most rapidly growing areas of investigation is the IT-SOFC.[21–24,27,28,34,35,42,43] Recently, ultrasonic spray pyrolysis with optimized process conditions has been used for obtaining nanostructured YSZ thin films, improving their electrical properties,[35] but conductivities are still low. The efficiency of this material as an electrolyte in SOFC can be increased using multilayer systems with nanostructured ceria-based materials.[18,26,28] But there are no reports of nanostructured ceria thin films obtained by this technique.

In this work, ultrasonic spray pyrolysis was used to deposit dense CeO_2 thin films with nanometric grain size. A study of the influence of different deposition parameters and the thermal annealing in the morphology of the films was made. The electrical properties of the films obtained were measured and compared with previous reports.

II. Experimental Procedure

The experimental setup shown in García-Sánchez et al.[35] was used. The diameter of the nozzle was 16 mm and the distance nozzle-substrate was fixed to 20 mm. Films were deposited onto (100) n-type, 200 $\Omega \cdot$ cm single crystalline silicon slices in order to perform electrical measurements at high temperatures. The substrates were ultrasonically cleaned, with trichloroethylene, acetone, methanol, and 5% HF solution in order to remove the native oxide. The spray solution was 0.025*M* of cerium (IV)

M. P. Paranthaman—contributing editor

Manuscript No. 26043. Received March 27, 2009; approved August 5, 2009.
This research was partially supported by the Projects PUNTA-UNAM, DGAPA IN-115708, and CONACYT-48970.
[†]Author to whom correspondence should be addressed. e-mail: mf@iim.unam.mx

acetylacetonate [$Ce(acac)_4 = Ce(C_5H_7O_2)_4$] from Sigma-Aldrich Chemicals, (México D.F., México) dissolved in anhydrous methanol. The additive's influence was studied by adding 1 mL of acetic acid (CH_3COOH) in 0.5 L of anhydrous methanol. The temperature of the heating plate (Ts) was controlled in the range of 325°–600°C, and the deposition time (t_d) was varied between 5 and 30 min. The carrier gas flow rate was fixed at 1.5 L/min and the director gas, air in both cases, was varied between 1 and 3.5 L/min.

The mass loss profile was registered by simultaneous thermogravimetric analysis (TGA) and differential scanning calorimety (DSC) (TA Instruments model SDT Q600 version 8.3, México D.F., México). The instrument control software ("Universal Analysis") was used to process the data. The heating rate was 5°C/min in a flow of air. The films were examined with field emission scanning electron microscopy (SEM) (XL 30 FEG/SIRION with focused ion- and electron-beam, energy-dispersive X-ray spectroscopy, and energy-dispersive angle X-ray GENESIS 4000). An atomic force microscope (AFM) (Jeol, JSPM-4210, México D.F., México) was used to analyze the surface of the samples. The crystalline structure was studied by X-ray diffraction (XRD) (Siemens D-500 diffractometer (México D.F., México) using the Cu$K\alpha$ wavelength (1.54056 Å)). The X-ray source was operated with a voltage of 25 kV and a current of 30 mA, to produce an intense X-ray beam whose incidence angle was 1°. The XRD spectra were obtained for 2θ angles in the range from 2° to 70° with steps of 0.020°. Considering the small thickness of the film, a long integration or step time (6.9 s) was used in order to obtain high-quality XRD spectra. Under these experimental conditions, the total acquisition time of each spectrum was around 11 h. The unit cell parameters were calculated using the Celref3 program.

Fourier-transformed infrared spectroscopy measurements (FTIR Nicolet Nexus 670, México D.F., México) demonstrated the absence of water in the films. The thickness of the films was measured with a profilometer (Sloan Dektac IIA, Tucson, AZ). For this purpose, a small part of the substrate was covered with a cover pyrex glass to form a step during deposition. The thickness of films was also measured by ellipsometry (Gaertner 117A ellipsometer, Skokie, IL) using the 633 nm line from a He–Ne laser. Both methods ellipsometry and profilometry indicated similar thickness values for films deposited at the same conditions. The room-temperature refractive index was calculated using the AUTOST program provided by the ellipsometer.

AC measurements were carried out using a Frequency Response Analyzer (Solartron 1260) over the range 0.1 Hz$<f<$10 MHz and for temperatures between 25° and 350°C. A parallel pattern of two gold electrodes was sputtered on the film surface to be used as electrodes.[3,35]

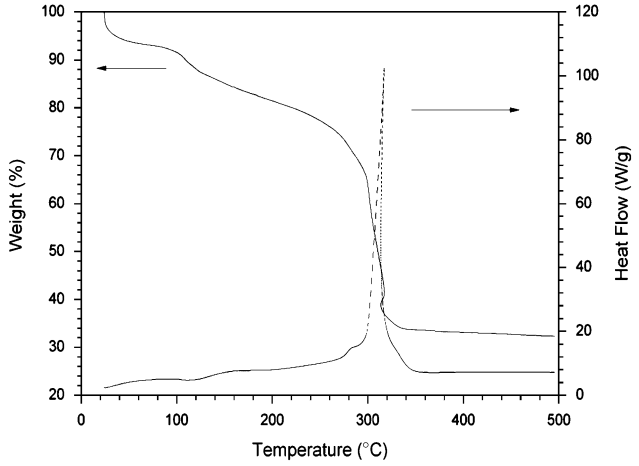

Fig. 1. Thermogravimetric and differential scanning calorimetric data for $Ce(acac)_4$ in air, 5°C/min.

III. Results and Discussion

(1) Thermal Analysis of Metal–Organic Precursors

The TG and DSC curves of metal–organic precursor obtained in air atmosphere are shown in Fig. 1. TGA curve shows three well-defined steps. The first two steps (weight loss of ~13%) start at room temperature and finish at approximately 120°C. These are attributed to water desorption. From 275° to 325°C, there is a rapid weight loss (of ~53%) and finally, decomposition of $Ce(acac)_4$ is completed at 342°C. The rapid loss is accompanied by a strong exothermic peak, which can be attributed to the decomposition of cerium acetylacetonate into oxides. The decomposition temperature of cerium acetylacetonate is thus found to be 342°C.

In spray pyrolysis, vaporization of the solvent occurs with the increase of droplets temperature while they gradually approach the surface of the substrate. Typical CVD characteristics are obtained in this method when the metal–organic precursor decomposes to metal oxides just above the substrate.[41] Then, the substrate temperature should be higher than the decomposition temperature of the precursors.[35,38,41] In this work, we chose 325°–600°C as the deposition temperatures for different films.

(2) Influence of Additives

SEM micrographs of the films grown during 10 min at 400°C with and without acetic acid are shown in Figs. 2(a) and (b), respectively. In films grown without additives, the presence of cracks is observed (Fig. 2(a)).

AFM images (supplementary information) show that the samples grown without additives present pores when either the temperature or time were varied. It is important to note that in the precursor solution of these samples, low solubility was also observed. This low solubility must be caused by the presence of water in the solution. Although anhydrous methanol is used, this solvent is hydrophilic, and the presence of water in cerium acetylacetonate was observed in thermal analysis in Fig. 1. The water in the solution produces cerium hydroxides, which have

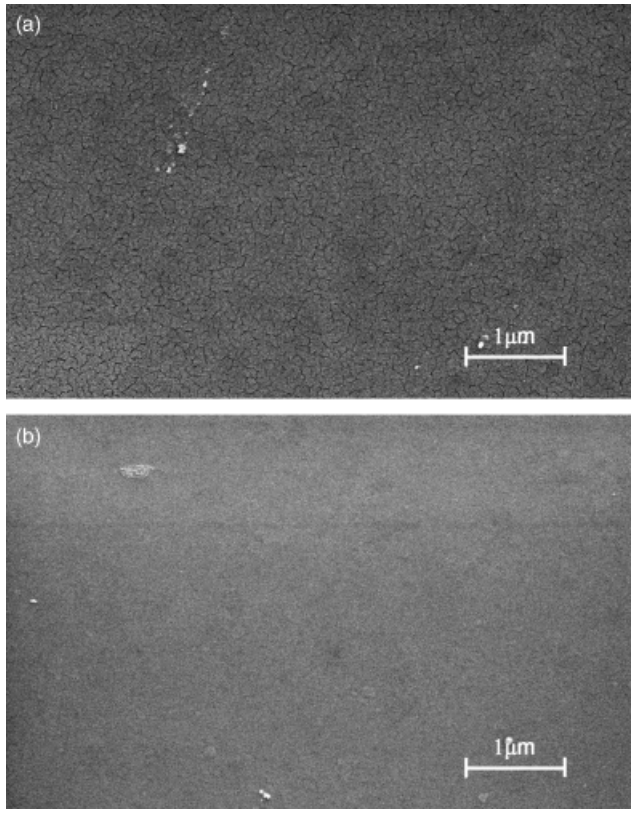

Fig. 2. Scanning electron microscopic images of films grown at 400°C for 10 min (a) without and (b) with additives.

low solubility and different decomposition temperature. Acetic acid avoids the formation of hydroxides, allowing the homogeneity of the solution and the formation of dense films (Fig. 2(b)).[44,45] In other materials too it has been observed that the presence of acetic acid changes the pH, the surface tension of solution and favors the formation of more homogeneous and smaller droplets.[44–47] Anyway, as crack-free samples are desired, additives were used in the solution for the rest of the samples.

(3) Influence of Substrate Temperature

SEM images (not shown) do not exhibit observable differences in samples grown at different temperatures for 10 min. The films have good adherence to substrates, and no cracks or detachments were observed, even for films deposited at low temperatures. It must be due to the small droplet size and the small flow rate of the carrier gas, which allows the evaporation of solvents from droplets before arriving to the substrate, avoiding additional stresses during the fast-drying process.[35] This is a very important factor considering the potential application of these films in SOFC or oxygen sensors.

However, in AFM images can be observed a more irregular surface with larger grain size (Fig. 3(a)) in the sample deposited at the lowest substrate temperature (325 °C). Although great splashes are not observed for the small size of droplets, the temperature of these samples is lower than the decomposition of precursor and the reaction occurs in the surface of the sample-forming spaced grains.[35,37] With the increase of temperature at 425 °C (Fig. 3(b)), a smooth surface is obtained indicating a CVD-like process.[41] The grain size was calculated increasing the magnification of SEM images and using the Digital Micrograph software.[35] An average grain size around 10 nm was estimated, in concordance with AFM results. The surface roughness (R_a) of the AFM scans in samples growth at these temperatures was lower than 0.4 nm, indicating a smooth surface. At higher temperatures, once again an irregular surface is obtained by the arrivial of dry droplets in the surface of the substrate (Fig. 3(c)).[35]

These results are in coincidence with the variations of refractive index with the substrate temperature (Fig. 4). It has been known that porosity decreases the refractive index of films.[4,5,9,15,48] In general, it has been reported that CeO_2 grown in a columnar structure with a high amount of pores in the structure, results in a low refractive index ($n<2$ for as-grown samples)[4,5,9,15] related to the bulk ($n = 2.36$[49] or 2.4[4]). In Fig. 4 is observed that the refractive index increases with the temperature of the substrate until 450°C, after which it remains constant. From the analysis of AFM results (Fig. 3(c)), it is expected that the refractive index decreases with the increase of porosity at higher temperatures. But the increase of experimental uncertainties at higher temperatures—due to the increased superficial roughness that scatters the laser signal—hinders a concluding result. Using the Lorentz–Lorentz law to relate the film density with the refractive index,[15,48] the relative density of the films at 425°C is 0.89. This value indicates a higher density than at obtained in other reports.[4,5,9,15] Then, 425°C was selected as the optimal substrate temperature.

(4) Influence of Flow Rates

When a liquid is subjected to a sufficiently high intensity of ultrasonic field, the splitting of liquid occurs to form droplets and they are ejected from the liquid interface into the surrounding air as a very fine dense fog. The flow rate of aerosol carrier gas adjusts the fog density varying the air flow passing over the liquid surface, an important factor to obtain homogeneous films.[50] This flow rate value was adjusted to 1.5 L/min to obtain a dense and constant fog. In the experimental system, a director gas was added, which allowed to increase the velocity of droplets arriving on the heated substrate, but in the same way reduced the time of approaching of droplets into the substrate.[35] The change of flow can also produce some droplets that join together to increase their size, and producing splashes in the surface of the film, as it is observed in Fig. 5 for a director gas flow rate of 3.5 L/min. Then, a director gas flow rate of 1.0 L/min was used in the rest of the samples.

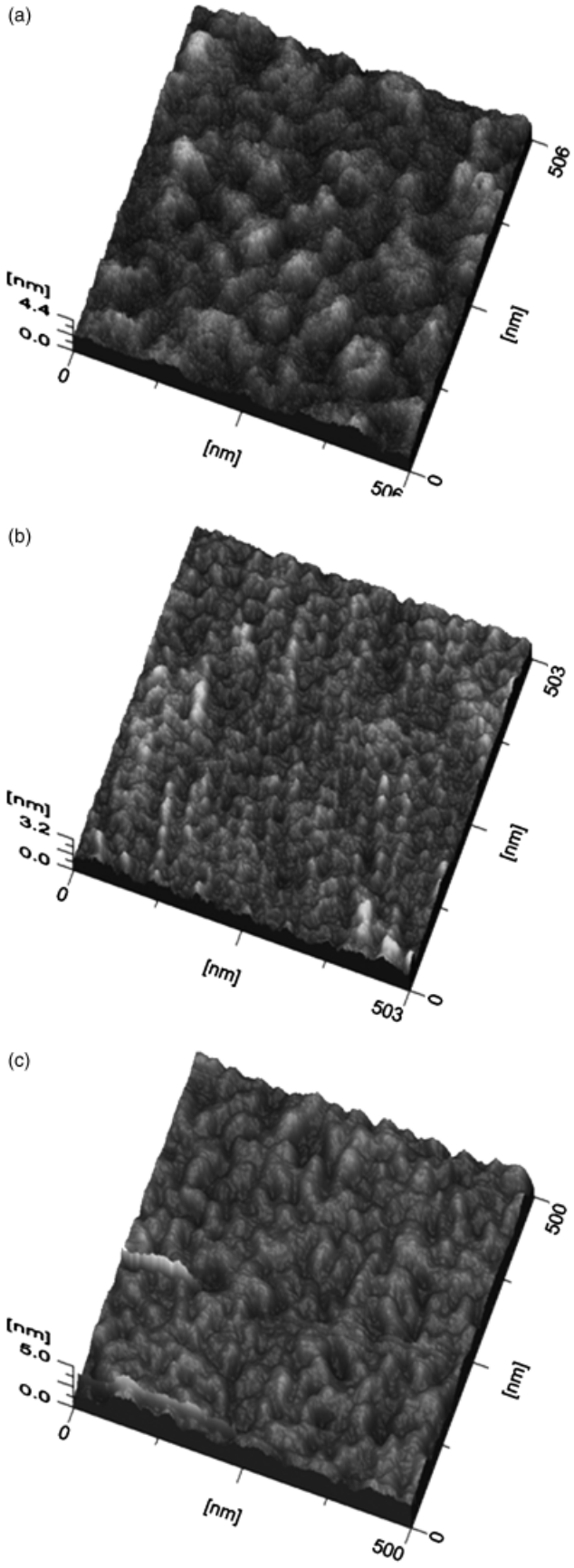

Fig. 3. Atomic force microscopic images of films grown at (a) 325°C, (b) 425°C, and (c) 600°C for 10 min.

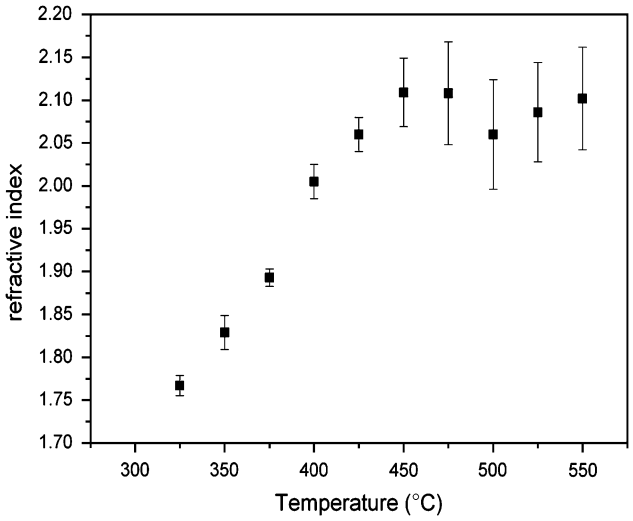

Fig. 4. Room temperature refractive index as a function of substrate temperature for film growth.

(5) Influence of the Deposition Time

An increase in deposition time does not produce important changes in the morphology of films.[4,32,35,39] Figure 6 shows the dependence of the thickness of the film deposited at 425°C as a function of deposition time. As it can be seen, the thickness of the film increases linearly with the deposition time. This shows that the film layer can be well adjusted, which is very important in technological applications. A similar result was found at the other substrate temperatures.

(6) Influence of Thermal Annealing

Considering that the decomposition temperature of $Ce(acac)_4$ is over 342°C (Fig. 1), CeO_2 films without organic residues must be expected in samples grown at temperatures higher than 350°C. Anyway, a thermal annealing at 600°C for 2 h, was conducted on to the films, considering that this temperature is close to the expected operating temperature of thin film fuel cell.[18] Figure 7 shows the results of XRD of a film grown at 425 °C with and without thermal annealing.

The XRD pattern shows that the film is crystalline in both cases, corresponding to cubic ceria (JCPDS file no. 34-0394) having a fluorite structure (space group *Fm3m*) and the second phases are not present.[2,3,12,30] The structure does not change with thermal annealing. No preferential orientation is observed in the XRD pattern in the direction of the substrate, but it is important to note that an amorphous silicon dioxide film of the

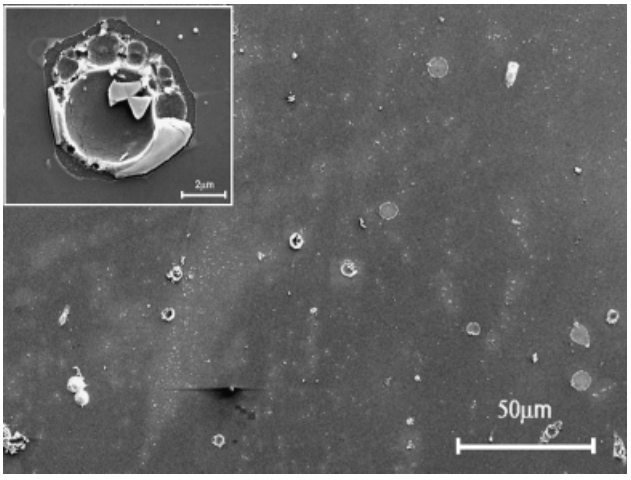

Fig. 5. Scanning electron microscopic image of film grown at 425°C with director gas flow rate of 3.5 L/min.

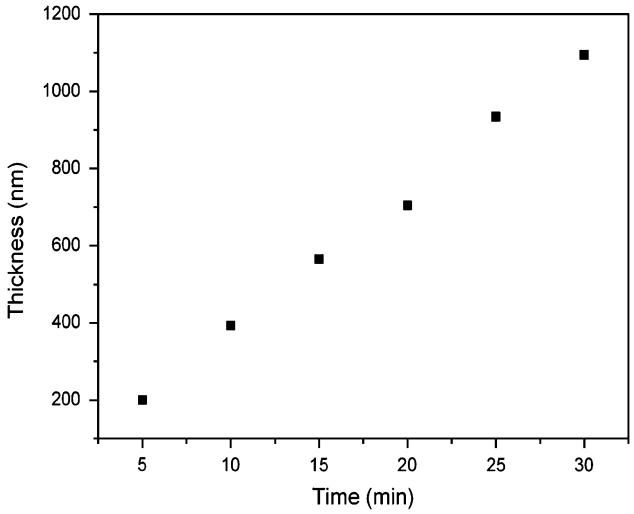

Fig. 6. Variation of thickness with deposition time in samples grown at 425 °C.

order of 10 nm is formed at the Si/CeO_2 interface after and during the growth process.[51,52] The lattice parameter (a), calculated from the peaks positions, is (0.5405 ± 0.0010) and (0.5418 ± 0.0013) nm for thermal treated and as-grown samples, respectively, in coincidence with the reported values.[2,3,6,7,11,12,29,30] The average crystallite sizes (D) were estimated from XRD patterns for the (200) peak, using the Scherrer formula corrected for instrument contribution, as

$$D = \frac{0.9\lambda}{\beta \cos \theta_B} \quad (1)$$

where λ is the wavelength of the incident beam, β is the intrinsic width at half maximum of the *hkl* line and θ_B is the Bragg diffraction angle. The crystallite sizes in as-grown and annealed samples were of 7.2 and 8.2 nm, respectively, in agreement with the measured values by SEM. As in previous reports, the crystallite size is higher in annealed samples.[35]

(7) Electrical Properties

The ac impedance measurements were carried out from 21° to 350°C for films grown at a substrate temperature of 425°C for 10 min. Figure 8 shows the behavior of a real part of conductivity vs. frequency at different temperatures.

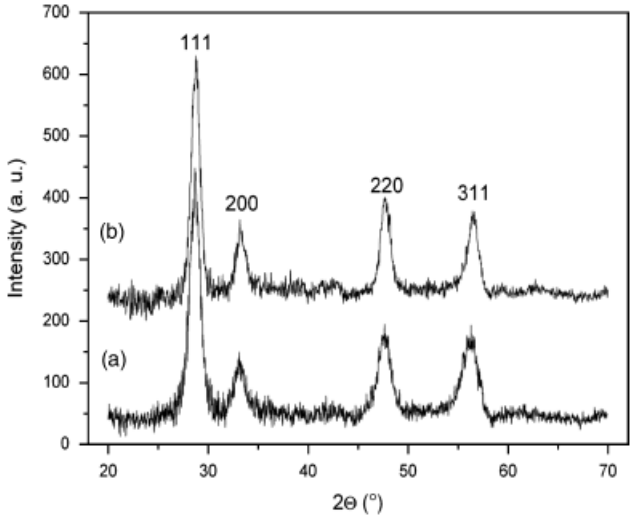

Fig. 7. X-ray diffraction plots of films grown at 425°C for 30 min (a) without and (b) with thermal annealing.

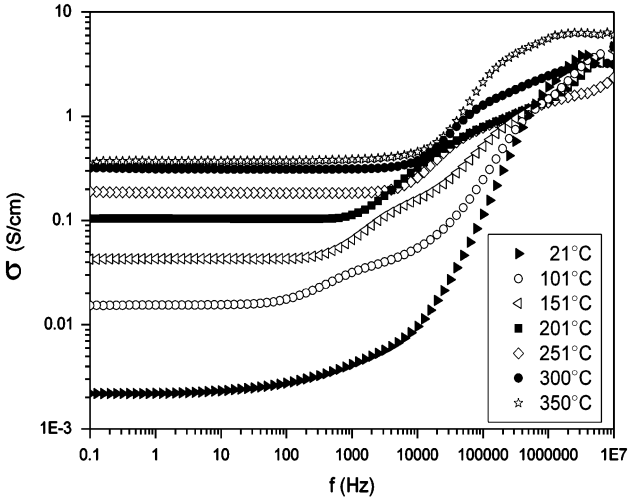

Fig. 8. An ac conductivity versus frequency at different temperatures.

At low frequencies, the conductivity shows almost no dependence on the frequency, corresponding to a dc conduction mechanism.[53] With the increase of frequency, a dispersion of conductivity is observed suggesting a power law. Next, the conductivity becomes constant again and forms another plateau. Finally, another dispersion is observed at higher frequencies that overlap with the plateau. Comparing with reports in CeO_2 thin films obtained by flash evaporation, the electrode response is not expected in this frequency range.[3] Then, the first dispersion can be associated to a grain boundary process and the other one to the response of grains. The capacity associated to these processes ($\sim 10^{-8}$ and $\sim 10^{-11}$ F, respectively) in an impedance complex plots confirms these results.[53] In this case, the dc conductivity is associated to the total response of the film, including grain and grain boundary behavior. The conductivity is increased in one order of magnitude with respect to that obtained by flash evaporation.[3] This result is attributed to dense and smooth films with nanometric size of grains obtained. Similar results were recently obtained in nanostructured YSZ thin films.[35]

The values of dc conductivity were measured at 1 Hz, because this frequency belongs, for all temperatures, to the frequency-independent interval of the ac response. The plot of log (σT) vs $1/T$ adjusts quite well to straight lines (Fig. 9), which indicates

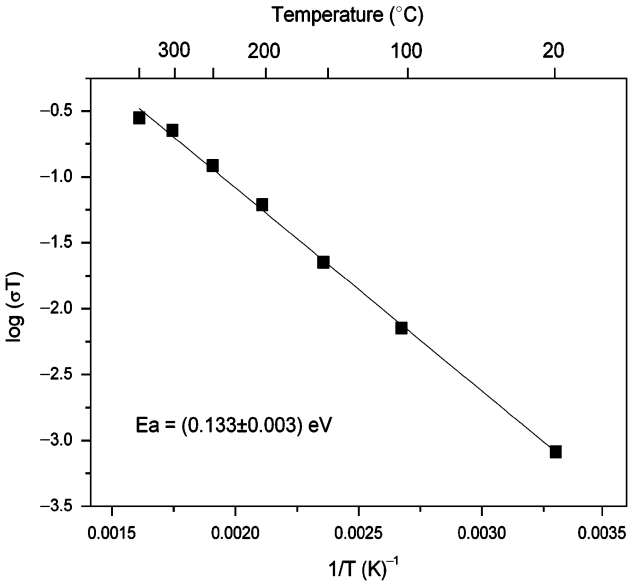

Fig. 9. Arrhenius ionic conductivity plots for total conductivity.

that the conductivity for all these samples can be expressed in the form of the Arrhenius relationship: $\sigma T = A \exp(-E_a/kT)$, where E_a is the activation energy for ion migration, A is the pre-exponetial factor, k is the Boltzmann constant, and T is the temperature in Kelvin. The activation energy (0.13 eV) is low with respect to other reports.[1–3,9,33] Porqueras *et al.*[9] report activation energy values between 0.28 eV and 0.1 eV in CeO_2 thin films deposited by e-beam PVD, when the temperature is below 100°C. But in that case, this low value is attributed to the loss of water in the heating process, which is not expected at the measurement temperatures in this work. Suzuki *et al.*[1] report an increase of defect concentration with the decrease of grain size. They obtain activation energy of 0.99 eV, but they conclude that the electrical conductivity of nanocrystalline CeO_2 is microstructure dependent, the activation energy decreases with the decreasing of grain size. Similar results were obtained by Rupp *et al.*[33] in gadolinia-doped ceria thin films, where the activation energy decreases linearly from 1.04 to 0.77 eV with a decreasing average grain size from 76 to 29 nm. Anyway, this is not a single phenomenon as the conducting species can be electrons or oxygen ions. Separation of ionic and electronic component using a method recently developed and the analysis of its influence in the total conductivity reported is now in progress.[54]

IV. Conclusions

Smooth, dense, and homogeneous CeO_2 films have been deposited in silicon substrates by ultrasonic spray pyrolysis. Acetic acid was added to the solution for obtaining crack-free films. The use of ultrasonic-generated mist and low concentration of precursor permitted to obtain small droplets. The decrease of droplets diameter allowed the use of low substrate temperature, increasing the deposition rate, and reducing the splashing residues on the surface. With these experimental conditions, nanostructured films with particles sizes <10 nm were produced. The conductivity of films is increased and the activation energy is reduced with the reduction of porosity and nanoparticles size, which is very important in low-temperature electrochemical devices based on CeO_2.

Acknowledgments

The authors acknowledge Dra. B. M. Monroy for the fruitful discussions and the technical assistance of E. Fregoso-Israel, C. Flores, L. Baños, A. Tejeda, O. Novelo, J. Camacho, O. Jiménez, and T. Vázquez of IIM-UNAM.

References

[1]T. Suzuki, I. Kosacki, H. U. Anderson, and P. Colomban, "Electrical Conductivity and Lattice Defects in Nanocrystalline Cerium Oxide Thin Films," *J. Am. Ceram. Soc.*, **84**, 2007–14 (2001).

[2]I. Kosacki, T. Suzuki, V. Petrovsky, and H. U. Anderson, "Electrical Conductivity of Nanocrystalline Ceria and Zirconia Thin Films," *Solid State Ion.*, **136–137**, 1225–33 (2000).

[3]A. Ramírez-Duverger, A. R. Ruiz-Salvador, M. P. Hernández-Sánchez, M. F. García-Sánchez, and G. Rodríguez-Gattorno, "CeO_2 Thin Films by Flash Evaporation," *Solid State Ion.*, **96**, 89–93 (1997).

[4]R. P. Netterfield, W. G. Sainty, P. J. Martin, and S. H. Sie, "Properties of CeO_2 Thin Films Prepared by Oxygen-Ion-Assisted Deposition," *Appl. Opt.*, **24**, 2267–72 (1985).

[5]S. Debnath, M. R. Islam, and M. S. R. Khan, "Optical Properties of CeO_2 Thin Films," *Bull. Mater. Sci.*, **30**, 315–9 (2007).

[6]N. Savvides, A. Thorley, S. Gnanarajan, and A. Katsaros, "Epitaxial Growth of Cerium Oxide Thin Film Buffer Layers Deposited by d.c. Magnetron Sputtering," *Thin Solid Films*, **388**, 177–82 (2001).

[7]B. Elidrissi, M. Addou, M. Regragui, C. Monty, A. Bougrine, and A. Kachouane, "Structural and Optical Properties of CeO_2 Thin Films Prepared by Spray Pyrolysis," *Thin Solid Films*, **379**, 23–7 (2000).

[8]S. Tsunekawa, T. Fukuda, and A. Kasuya, "Blue Shift in Ultraviolet Absorption Spectra of Monodisperse CeO_{2-x} Nanoparticles," *J. Appl. Phys.*, **87**, 1318–21 (2000).

[9]I. Porqueras, C. Person, and E. Bertran, "Influence of the Film Structure on the Properties of Electrochromic CeO_2 Thin Films Deposited by e-Beam PVD," *Thin Solid Films*, **447–448**, 119–24 (2004).

[10]R. Jose, V. Thavasi, and S. Ramakrishna, "Metal Oxides for Dye-Sensitized Solar Cells," *J. Am. Ceram. Soc.*, **92**, 289–301 (2009).

[11]N. L. Petrova, R. V. Todorovska, and D. S. Todorovsky, "Spray-Pyrolysis Deposition of CeO_2 Thin Films Using Citric or Tartaric Complexes as Starting Materials," *Solid State Ion.*, **177**, 613–21 (2006).
[12]K. Konstantinov, I. Stambolova, P. Peshev, B. Darriet, and S. Vassilev, "Preparation of Ceria Films by Spray Pyrolysis Method," *Int. J. Inorg. Mater.*, **2**, 277–80 (2000).
[13]S. Wang, W. Wang, Q. Liu, M. Zhang, and Y. Qian, "Preparation and Characterization of Cerium (IV) Oxide Thin Films by Spray Pyrolysis Method," *Solid State Ion.*, **133**, 211–5 (2000).
[14]M. Wei and K. L. Choy, "Deposition of Cerium Oxide Films on Si (100) and Glass Substrates Using the ESAVD Method," *J. Cryst. Growth*, **284**, 464–9 (2005).
[15]S. M. A. Durrani, M. F. Al-Kuhaili, and I. A. Bakhtiari, "Carbon Monoxide Gas-Sensing Properties of Electron-Beam Deposited Cerium Oxide Thin Films," *Sens. Actuators B*, **134**, 934–9 (2008).
[16]P. Jasinski, T. Suzuki, and H. U. Anderson, "Nanocrystalline Undoped Ceria Oxygen Sensor," *Sens. Actuators B*, **95**, 73–7 (2003).
[17]Q. N. Minh, "Ceramic Fuel Cells," *J. Am. Ceram. Soc.*, **76**, 563–88 (1993).
[18]D. Perednis and L. J. Gauckler, "Solid Oxide Fuel Cells with Electrolytes Prepared Via Spray Pyrolysis," *Solid State Ion.*, **166**, 229–39 (2004).
[19]J. L. M. Rupp, T. Drobek, A. Rossi, and L. J. Gauckler, "Chemical Analysis of Spray Pyrolysis Gadolinia-Doped Ceria Electrolyte Thin Films for Solid Oxide Fuel Cells," *Chem. Mater.*, **19**, 1134–42 (2007).
[20]J.-C. Chen and B.-H. Hwang, "Microstructure and Properties of the Ni–CGO Composite Anodes Prepared by the Electrostatic-Assisted Ultrasonic Spray Pyrolysis Method," *J. Am. Ceram. Soc.*, **91**, 97–102 (2008).
[21]V. Esposito and E. Traversa, "Design of Electroceramics for Solid Oxides Fuel Cell Applications: Playing with Ceria," *J. Am. Ceram. Soc.*, **91**, 1037–51 (2008).
[22]Y.-P. Fu, S.-B. Wen, and C.-H. Lu, "Preparation and Characterization of Samaria-Doped Ceria Electrolyte Materials for Solid Oxide Fuel Cells," *J. Am. Ceram. Soc.*, **91**, 127–31 (2008).
[23]B. P. Gorman and H. U. Anderson, "Processing of Composite Thin Film Solid Oxide Fuel Cell Structures," *J. Am. Ceram. Soc.*, **88**, 1747–53 (2005).
[24]Y. Liu, B. Li, X. Wei, and W. Pan, "Citric-Nitrate Combustion Synthesis and Electrical Conductivity of the Sm^{3+} and Nd^{3+} Co-Doped Ceria Electrolyte," *J. Am. Ceram. Soc.*, **91**, 3926–30 (2008).
[25]N. Oishi, A. Atkinson, N. P. Brandon, J. A. Kilner, and B. C. H. Steele, "Fabrication of an Anode-Supported Gadolinium-Doped Ceria Solid Oxide Fuel Cell and Its Operation at 550°C," *J. Am. Ceram. Soc.*, **88**, 1394–6 (2005).
[26]J.-Y. Park, H. Yoon, and E. D. Wachsman, "Fabrication and Characterization of High-Conductivity Bilayer Electrolytes for Intermediate-Temperature Solid Oxide Fuel Cells," *J. Am. Ceram. Soc.*, **88**, 2402–8 (2005).
[27]S. Suda, K. Kawahara, M. Kawano, H. Yoshida, and T. Inagaki, "Preparation of Matrix-Type Nickel Oxide/Samarium-Doped Ceria Composite Particles by Spray Pyrolysis," *J. Am. Ceram. Soc.*, **90**, 1094–100 (2007).
[28]L. Zhang, H. Q. He, W. R. Kwek, J. Ma, E. H. Tang, and S. P. Jiang, "Fabrication and Characterization of Anode-Supported Tubular Solid-Oxide Fuel Cells by Slip Casting and Dip Coating Techniques," *J. Am. Ceram. Soc.*, **92**, 302–10 (2009).
[29]G. Linker, R. Smithey, J. Geerk, F. Ratzel, R. Schneider, and A. Zaitsev, "The Growth of Ultra-Thin Epitaxial CeO_2 Films on *r*-Plane Sapphire," *Thin Solid Films*, **471**, 320–7 (2005).
[30]M. Pan, G. Y. Meng, H. W. Xin, C. S. Chen, D. K. Peng, and Y. S. Lin, "Pure and Doped CeO_2 Thin Films Prepared by MOCVD Process," *Thin Solid Films*, **324**, 89–93 (1998).
[31]R. Aguiar, F. Sánchez, C. Ferrater, and M. Varela, "Protective Oxide Coatings for Superconducting $YBa_2Cu_3O_{7-x}$ Thin Films," *Thin Solid Films*, **306**, 74–7 (1997).
[32]T. Chaudhuri, S. Phok, and R. Bhattacharya, "Pulsed-Laser Deposition of Textured Cerium Oxide Thin Films on Glass Substrates at Room Temperature," *Thin Solid Films*, **515**, 6971–4 (2007).
[33]J. L. M. Rupp and L. J. Gauckler, "Microstructures and Electrical Conductivity of Nanocrystalline Ceria-Based Thin Films," *Solid State Ion.*, **177**, 2513–8 (2006).
[34]J. L. M. Rupp, A. Infortuna, and L. J. Gauckler, "Thermodynamic Stability of Gadolinia-Doped Ceria Thin Film Electrolytes for Micro-Solid Oxide Fuel Cells," *J. Am. Ceram. Soc.*, **90**, 1792–7 (2007).
[35]M. F. García-Sánchez, J. Peña, A. Ortiz, G. Santana, J. Fandiño, M. Bizarro, F. Cruz-Gandarilla, and J. C. Alonso, "Nanostructured YSZ Thin Films for Solid Oxide Fuel Cells Deposited by Ultrasonic Spray Pyrolysis," *Solid State Ion.*, **179**, 243–9 (2008).
[36]D. Perednis, O. Wilhelm, S. E. Pratsinis, and L. J. Gauckler, "Morphology and Deposition of Thin Yttria-Stabilized Zirconia Films Using Spray Pyrolysis," *Thin Solid Films*, **474**, 84–95 (2005).
[37]R. Neagu, D. Perednis, A. Princivalle, and E. Djurado, "Initial Stages in Zirconia Coatings Using ESD," *Chem. Mater.*, **17**, 902–10 (2005).
[38]O. Wilhelm, S. E. Pratsinis, D. Perednis, and L. J. Gauckler, "Electrospray and Pressurized Spray Deposition of Yttria-Stabilized Zirconia Films," *Thin Solid Films*, **479**, 121–9 (2005).
[39]Y. Matsuzaki, M. Hishinuma, and I. Yasuda, "Growth of Yttria Stabilized Zirconia Thin Films by Metallo-Organic, Ultrasonic Spray Pyrolysis," *Thin Solid Films*, **340**, 72–6 (1999).
[40]E. Ramírez, A. Huanosta, J. Sebastian, L. Huerta, A. Ortiz, and J. C. Alonso, "Structure, Composition and Electrical Properties of YSZ Films Deposited by Ultrasonic Spray Pyrolysis," *J. Mater. Sci.*, **42**, 901–7 (2007).
[41]H. Song, C. Xia, Y. Jiang, G. Meng, and D. Peng, "Deposition of Y_2O_3 Stabilized ZrO_2 Thin Films from $Zr(DPM)_4$ and $Y(DPM)_3$ by Aerosol-Assisted MOCVD," *Mater. Lett.*, **57**, 3833–8 (2003).
[42]P. Lenormand, M. Rieu, R. F. Cienfuegos, P. A. Julbe, S. Castillo, and F. Ansart, "Potentialities of the Sol–Gel Route to Develop Cathode and Electrolyte Thick Layers: Application to SOFC Systems," *Surf. Coat. Technol.*, **203**, 901–4 (2008).
[43]P. Muralidharan, S. H. Jo, and D. K. Kim, "Electrical Conductivity of Submicrometer Gadolinia-Doped Ceria Sintered at 1000°C Using Precipitation-Synthesized Nanocrystalline Powders," *J. Am. Ceram. Soc.*, **91**, 3267–74 (2008).
[44]C. H. Chen, E. M. Kelder, and J. Schoonman, "Effects of Additives in Electrospraying for Materials Preparation," *J. Eur. Ceram. Soc.*, **18**, 1439–43 (1998).
[45]L. Castañeda, A. García-Valenzuela, E. P. Zironi, J. Cañetas-Ortega, M. Terrones, and A. Maldonado, "Formation of Indium-Doped Zinc Oxide Thin Films Using Chemical Spray Techniques: The Importance of Acetic Acid Content in the Aerosol Solution and the Substrate Temperature for Enhancing Electrical Transport," *Thin Solid Films*, **503**, 212–8 (2006).
[46]P. Lutz Mädler and S. E. Pratsinis, "Bismuth Oxide Nanoparticles by Flame Spray Pyrolysis," *J. Am. Ceram. Soc.*, **85**, 1713–18 (2002).
[47]A. Maldonado, R. Asomoza, J. Cañetas-Ortega, E. P. Zironi, R. Hernández, R. Patiño, and O. Solorza-Feria, "Effect of the pH on the Physical Properties of ZnO: In Thin Films Deposited by Spray Pyrolysis," *Sol. Ener. Mater. Sol. Cells*, **57**, 331–44 (1999).
[48]M. Harris, H. A. Macleod, S. Ogura, E. Pelletier, and B. Vidal, "The Relationship between Optical Inhomogeneity and Film Structure," *Thin Solid Films*, **57**, 173–8 (1979).
[49]D. R. Shannon, C. R. Shannon, O. Medenbach, and X. R. Fischer, "Refractive Index and Dispersion of Fluorides and Oxides," *J. Phys. Chem. Ref. Data*, **31**, 931–70 (2002).
[50]R. Rajan and A. B. Pandit, "Correlations to Predict Droplet Size in Ultrasonic Atomisation," *Ultrasonics*, **39**, 235–55 (2001).
[51]H. F. Wolf, *Semiconductors*, pp. 342–62. Wiley–Interscience, New York, 1971.
[52]L. E. Katz, "Oxidation"; pp. 98–140 in *VLSI Technology*, Edited by S. M. Sze. McGraw-Hill Book Co, New York, 1988.
[53]M. F. García-Sánchez, J.-C. M'Peko, A. R. Ruiz-Salvador, G. Rodríguez-Gattorno, Y. Echevarría, F. Fernández-Gutierrez, and A. Delgado, "An Elementary Picture of Dielectric Spectroscopy in Solids: Physical Basis," *J. Chem. Educ.*, **80**, 1062–73 (2003).
[54]M.-F. García-Sánchez, N. Fernández, M.-L. Martínez-Sarrion, L. Mestres, F. Fernández-Gutierrez, G. Santana, and A. R. Ruiz-Salvador, "Separation of Electronic and Ionic Conductivity in Mixed Conductors from the AC Response: Application to $Pr_{0.56}Bi_{0.04}Li_{0.2}TiO_3$," *Appl. Phys. Lett.*, **93**, 034105, 3pp (2008). □